Time-Dependent (Current) Density Functional Theory for Periodic Systems

Kootstra, F.; Boeij, P.L. de; Leeuwen, R. van; Snijders, J.G.

Published in:
EPRINTS-BOOK-TITLE

Publication date:
2002

CHAPTER 1

TIME-DEPENDENT (CURRENT) DENSITY FUNCTIONAL THEORY FOR PERIODIC SYSTEMS

F. Kootstra, P. L. de Boeij, R. van Leeuwen, and J. G. Snijders

Theoretical Chemistry, Materials Science Centre
Rijksuniversiteit Groningen
Nijenborgh 4, 9747 AG Groningen
The Netherlands
E-mail: F.Kootstra@chem.rug.nl

In this article we review time-dependent density functional theory for calculating the static and frequency-dependent dielectric function $\epsilon(\omega)$ of nonmetallic crystals. We show that a real-space description becomes feasible for solids by using a combination of a lattice-periodic (microscopic) scalar potential with a uniform (macroscopic) electric field for the description of the effective one-electron system. We treat the time-dependent fields as perturbations in a periodic structure calculation. The induced density and microscopic potential can be obtained self-consistently for fixed macroscopic field by using linear response theory in which Coulomb interactions and exchange-correlation effects are included. The dielectric function can then be obtained from the induced current. We obtained $\epsilon(\omega)$ for a wide variety of nonmetallic crystals within the adiabatic local density approximation (ALDA) in good agreement with experiment. In particular in the low-frequency range no adjustment of the band gap obtained within the local density approximation (LDA) seems to be necessary. Relativistic effects on the dielectric response have been found to be important for a few semimetals that have inverted bandstructures within the LDA. Exchange-correlation effects beyond the ALDA have been treated by a polarization-dependent functional for the effective electric field, with improved dielectric functions as result.

Contents

1. Introduction

In the early 1960's Hohenberg and Kohn [1] formulated the fundamental theorems of density functional theory (DFT) for the description of the ground state of a many-electron system in an external potential. This theory proved to be very practical after Kohn and Sham [2] incorporated it in a self-consistent field (SCF) calculation scheme for an effective one-electron system. This method has nowadays become one of the standard tools for the first-principle calculation of the properties of solids [3], and later also for atoms and molecules [4,5,6]. The accuracy of the results obtained with these methods is very good for a wide variety of ground state properties. Amongst the few exceptions the most prominent is the large deviation for the energy gap and the dielectric constant in semiconductors and insulators. The value for the dielectric constant obtained within the local density approximation (LDA) is usually overestimated by more than 10% [7,8]. A similar overestimation has been found for the static polarizabilities of atoms [9].

In the case of atoms and molecules, it was shown that inclusion of the correct asymptotic behavior of the exchange-correlation potential [10] greatly improves the results for the polarizabilities [11]. Since this correction affects mainly the contribution of the outer region, it seems to be less important

for larger molecules [11]. Therefore, we should not expect large deviations due to the neglect of such asymptotic corrections in the LDA results in solids.

In solids the discrepancy for the dielectric constant is often attributed to the mismatch between the Kohn-Sham energy gap and the gap as observed in optical spectra. Within LDA one typically underestimates the gap by 30%-50%. Attempts to improve these results by improving the quality of the various approximations for the exchange-correlation functional have had limited success. For instance, the inclusion of gradient corrections to the LDA reduces the error only slightly [12,13]. The error in the Kohn-Sham energy gap can be attributed to a discontinuity in the DFT exchange-correlation potential [14,15] and it is commonly believed that the gap has to be corrected by a near-rigid shift of the virtual states in order to get good results for the quasiparticle energies and dielectric constant [8,16,17,18]. There is, however, no formal justification within DFT for this so-called scissors operator [13]. In most materials, one has to use different shifts to match the excitation spectrum than to get a correct dielectric constant [18].

Gonze, Ghosez, and Godby [19] have indicated that this scissors-operator is an approximate way to deal with the special role of macroscopic polarization in these infinite systems. They made the remark that the original assumptions of Hohenberg and Kohn, are no longer valid in periodic systems, and that in principle the density must be supplemented with the macroscopic polarization in order to describe these systems completely.

The time-dependent extension of DFT, (TDDFT) rigorously proven in the 1980's by Runge and Gross [20], gave some new impetus to this field of research. Whereas ordinary DFT was formulated originally only for the (nondegenerate) ground state, Runge and Gross showed that the validity of the theorems could be extended to cover systems in *time-dependent* scalar potentials as well. The application of this theory to atoms and molecules proved to be very successful, e.g., the calculated response properties and excitation energies were greatly improved [11,21,22,23]. Ghosh and Dhara [24,25] showed that TDDFT also applies to systems which are being subjected to the more general time-dependent electromagnetic fields, in which case both the density and the current density are needed to fully describe the system. We will follow their description and derive an expression for the macroscopic polarization from the current density.

In this article we review the real-space description [26,27] of the self-

consistent field approach to TDDFT in solids, This computational scheme is similar to the density-functional perturbation scheme of Baroni *et al.* [28]. Most other implementations of TDDFT for solids use pseudopotentials in combination with a plane-wave basis [7,8,16]. This combination facilitates the description for the induced properties, like density and induced fields in Fourier space [29,30]. Self-consistency is achieved in a method which needs the construction of various response kernels as large matrix representations on this plane-wave basis, and for which one usually has to invert these matrices [7,31]. High accuracy can only be achieved at the expense of huge computation costs. The real-space description, however, is in efficiency comparable to ordinary ground-state calculations. We outline the main methodological features of the implementation, which is an extension to the full-potential linear combination of atomic orbitals (LCAO) code ADF-BAND [32,33]. This method has been applied to various nonmetallic crystals. We give an overview of the results for the dielectric constants, and the dielectric functions for several insulators and semiconductors [26,27]. We show how relativistic effects can be incorporated into this scheme, and we give the results for the materials InSb and HgSe that turn into semimetals within the LDA upon inclusion of scalar relativistic effects [34,35]. Finally we discuss the results for a polarization-dependent exchange-correlation functional [36] that has been derived form the current-dependent exchange-correlation functional of Vignale and Kohn [37].

2. Dielectric Response of Crystals

The theory of the dielectric properties of solids describes the linear response of crystals to externally applied electric fields. Therefore one has to treat macroscopically large systems in the presence of externally applied perturbing fields. The central problem in this theory is how to model real systems that are large but nevertheless finite using idealized periodic crystals of infinite extent. This connection can only be established by considering the proper asymptotic limit of finite systems to infinite size. There are two major problems to overcome; one has to find a proper definition of polarization in extended systems, and one has to deal with the sample-shape dependent electrical field of polarized media. In this section we give the proper definition for the macroscopic polarization. We show that it is important to identify macroscopic and microscopic contributions to the electric field and polarization. We have to do this in such a way that surface and sample-

shape dependent contributions can be separated from the bulk-intrinsic parts.

2.1. *Induced Macroscopic Polarization*

Before we formulate our microscopic treatment, let us recall the definitions for the macroscopic electric field $\mathbf{E}_{mac}(\mathbf{r},t)$ and the macroscopic polarization $\mathbf{P}_{mac}(\mathbf{r},t)$. Without losing generality we can consider the time-dependence to be harmonic with frequency ω. One commonly defines the macroscopic field at a point $\mathbf{r}$ inside the bulk as the average field that a test charge would experience in a region $\Omega_{\mathbf{r}}$ surrounding the point $\mathbf{r}$. This region must have a size d that is small compared to the wavelength $\lambda = 2\pi c/\omega$, but it nevertheless has to contain a large number of bulk unit cells; i.e., $\lambda \gg d \gg a$, where a is the lattice parameter. We thus define,

$$\mathbf{E}_{mac}(\mathbf{r},t) = \frac{1}{|\Omega_{\mathbf{r}}|}\int_{\Omega_{\mathbf{r}}} (\mathbf{E}_{ext}(\mathbf{r}',t) + \mathbf{E}_{ind}(\mathbf{r}',t))\, d\mathbf{r}'. \tag{1}$$

This macroscopic field contains the externally applied electric field plus the macroscopic part of the induced field. This induced field is the result of the reaction of the system to the external field.

Similarly the induced macroscopic polarization can be defined as the time-integral of the average induced current flowing in this region $\Omega_{\mathbf{r}}$,

$$\mathbf{P}_{mac}(\mathbf{r},t) = -\frac{1}{|\Omega_{\mathbf{r}}|}\int^{t}\int_{\Omega_{\mathbf{r}}} \delta\mathbf{j}(\mathbf{r}',t')\, d\mathbf{r}'\, dt', \tag{2}$$

where $\delta\mathbf{j}(\mathbf{r},t)$ is the induced current density. Note that the induced polarization is defined up to an (irrelevant) arbitrary constant. The definition for this macroscopic polarization becomes equivalent to the in general ill-defined but more common notion of 'an induced average dipole moment per unit volume,' only in systems where we can define the volume $\Omega_{\mathbf{r}}$ such that no currents flow across its boundary. The polarization given here is well-defined and model independent, i.e. , we do not have to satisfy such a boundary condition, and the value obtained is not depending on the particular choice for the unit cell of the periodic system. Note that both definitions Eqs. (1, and 2) are valid in finite and infinite systems.

Inside the bulk the macroscopic polarization is related to the macroscopic electric field rather than to the externally applied field, via what is

called the constitutive equation,

$$\mathbf{P}_{mac}(\mathbf{r},t) = \int^{t} \chi_e(t-t') \cdot \mathbf{E}_{mac}(\mathbf{r},t')\, dt'. \tag{3}$$

This equation defines the material property $\chi_e(\tau)$ called the electric susceptibility, from which the macroscopic dielectric function $\epsilon(\tau)$ is derived,

$$\epsilon(\tau) = 1 + 4\pi\chi_e(\tau). \tag{4}$$

In general $\chi_e(\tau)$ and $\epsilon(\tau)$ are tensors, which, however, simplify to scalars in isotropic systems.

2.2. *Periodic Model System*

In order to be able to derive these material properties, we have to give a microscopic account of the macroscopic contributions to the electric field and polarization for an arbitrary but fixed region $\mathcal{B}_{\mathbf{r}}$ inside the bulk. We therefore identify in the interior of the sample a large number of identical but otherwise arbitrary bulk unit cells, each having the same volume $|V|$. The cells which comprise the region $\mathcal{B}_{\mathbf{r}}$ will be enumerated using the indices i and are denoted by V_i.

Within the long-wavelength limit we can assume that in these cells both the induced charge and current distributions become lattice periodic. Hence the macroscopic field component becomes uniform throughout $\mathcal{B}_{\mathbf{r}}$. Under these conditions all relevant properties become lattice periodic so we can obtain the response of the region $\mathcal{B}_{\mathbf{r}}$ by using a model system with periodic boundary conditions.

However, we cannot obtain the electric field by simply evaluating the contributions of the lattice-periodic sources. Only the microscopic part can be obtained using the periodic lattice. The macroscopic component depends also on the external field and the sample shape, which are no longer properly defined in the periodic - hence infinite - model system. Instead we can consider the uniform macroscopic field for the periodic model system to be fixed. We will now construct the microscopic and macroscopic (scalar and vector) potentials which are due to the induced sources, and we will show that they lead to microscopic and macroscopic fields, respectively.

2.3. *Microscopic Potential*

For any finite region $\mathcal{B}_\mathbf{r}$ we can define the scalar potential $\delta v(\mathbf{r},t)$ of the induced density $\delta\rho(\mathbf{r},t) = \rho(\mathbf{r},t) - \rho_0(\mathbf{r})$. The action is instantaneous within the Coulomb gauge, so the potential follows from [a],

$$\delta v(\mathbf{r},t) = \int_{\mathcal{B}_\mathbf{r}} \frac{\delta\rho(\mathbf{r}',t)}{|\mathbf{r}-\mathbf{r}'|}\, d\mathbf{r}'. \tag{5}$$

It is well-established that this potential is not properly defined in the limit of $|\mathcal{B}_\mathbf{r}|$ to infinite size. In the periodic model system this ambiguity arises due to the divergent and conditionally convergent lattice sum contributions of the monopole, dipole, and quadrupole moments of the density in the cells V_i.

We can, however, define the microscopic component of this Coulomb potential by removing these conditionally convergent contributions. Therefore we construct for each unit cell V_i a uniform monopole, dipole and quadrupole density, and we subtract their contributions $\delta v_i(\mathbf{r},t)$ from the bare Coulomb potential of Eq. (5) according to,

$$\delta v_{mic}(\mathbf{r},t) = \sum_i \left(\int_{V_i} \frac{\delta\rho(\mathbf{r}',t)}{|\mathbf{r}-\mathbf{r}'|}\, d\mathbf{r}' - \delta v_i(\mathbf{r},t) \right). \tag{6}$$

The summation is over all cells V_i in the region $\mathcal{B}_\mathbf{r}$. The potential $\delta v_i(\mathbf{r},t)$ is defined as,

$$\delta v_i(\mathbf{r},t) = \int_{V_i} \sum_{n=0}^{2} \frac{1}{n!}\, \delta\mu^{(n)}_{i,j_1\cdots j_n}(t) \cdot \frac{\partial}{\partial r'_{j_1}} \cdots \frac{\partial}{\partial r'_{j_n}} \frac{1}{|\mathbf{r}-\mathbf{r}'|}\, d\mathbf{r}'. \tag{7}$$

In this expression we have implied a summation over all Cartesian components j_1 through j_n of the uniform multipole density of rank n, which are denoted by $\delta\mu^{(n)}_i(t)$. These uniform densities have to be constructed carefully in order to ensure that the conditionally convergent terms of Eq. (5) are exactly canceled in Eq. (6). Their value can be obtained for each cell V_i by requiring that all three leading-order terms in the multipole expansion of the contribution of this cell to the microscopic potential of Eq. (6) must vanish. We choose to represent these moments with respect to the geometric centers, i.e., with respect to $\mathbf{R}_i = (1/|V|)\int_{V_i} \mathbf{r}'\, d\mathbf{r}'$. The monopole density has to vanish in the periodic system due to the condition of charge neutrality. One can easily check that the uniform dipole and quadrupole densities

[a] we will use atomic units ($e = \hbar = m = 1$) throughout this article

can then be obtained from the average dipole and quadrupole moments of the unit cells,

$$\delta\mu_i^{(n)}(t) = \frac{1}{|V|}\int_{V_i} \delta\rho(\mathbf{r}',t)(\mathbf{r}'-\mathbf{R}_i)^n\, d\mathbf{r}', \tag{8}$$

where on the right-hand side the n^{th} tensor product is meant. Due to the periodicity these multipole densities are identical for each cell, so we can drop the index i in the sequel.

By removing the conditionally convergent terms in this way, the series of Eq. (6) becomes nicely convergent. If we choose $\mathcal{B}_\mathbf{r}$ finite but nevertheless sufficiently large, so that convergence is reached within $\mathcal{B}_\mathbf{r}$, we have established a proper definition for the microscopic potential for both periodic and finite systems.

On the other hand, the macroscopic potential can only be defined for the true, finite system. It forms the remainder of the bare Coulomb potential after the microscopic part has been removed. The terms $\delta v_i(\mathbf{r},t)$ (which were not included in the microscopic contribution of region $\mathcal{B}_\mathbf{r}$) have to be included in the macroscopic part of the potential,

$$\delta v_{mac}(\mathbf{r},t) = \int' \frac{\delta\rho(\mathbf{r}',t)}{|\mathbf{r}-\mathbf{r}'|}\, d\mathbf{r}' + \sum_i \delta v_i(\mathbf{r},t). \tag{9}$$

Here the integration domain in the first term on the right-hand side is the whole (finite) system, however, with the exclusion of the region $\mathcal{B}_\mathbf{r}$. This is indicated by the prime on the integral sign. The contribution of $\mathcal{B}_\mathbf{r}$ is given by the potential of the uniform multipole densities. Note that the resulting macroscopic potential comprises all surface and sample-shape dependent contributions, but excludes the microscopic contributions from the region $\mathcal{B}_\mathbf{r}$.

The uniform dipole and quadrupole sources in the region $\mathcal{B}_\mathbf{r}$ can equally well be represented using surface excess monopole and dipole layers at the boundary of $\mathcal{B}_\mathbf{r}$. Being remote, these can only lead to smooth, i.e. macroscopic fields at $\mathbf{r}$. A similar analysis holds for a uniform monopole density in $\mathcal{B}_\mathbf{r}$. Although this density has to vanish in the periodic model system, a macroscopic density fluctuating on a wavelength scale can exist in the finite system. However, such a slowly varying density can only lead to macroscopic fields. The microscopic potential, on the other hand, is lattice periodic, and can only lead to microscopic fields.

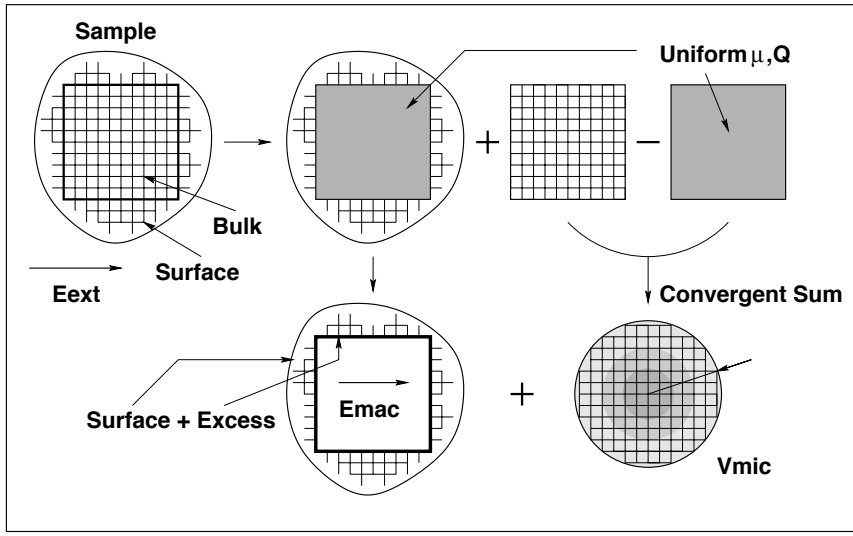

Fig. 1. The construction of the macroscopic electric field E_{mac} and the microscopic Coulomb potential v_{mic} for a dielectric sample in an external field. The bulk region $\mathcal{B}_r$ is removed from the sample and replaced by a uniformly polarized medium. The difference between the true bulk and this substitute leads to a microscopic potential. The field produced inside the uniform medium is equivalent to the field produced by additional excess surface charges. In combination with the surface region this yields the macroscopic field.

The result of the separation into microscopic and macroscopic contributions is that we are now able to evaluate the microscopic component of the Coulomb potential using the periodic model system. The construction sketched above is visualized in Fig. 1. The summation of Eq. (6) is nicely convergent, since contributions fall off sufficiently fast such that remote cells do not contribute. For its evaluation we can make use of an efficient screening technique [26], which weighs the contributions of the individual cells such that it leaves nearby cells unchanged, but removes remote cells explicitly.

2.4. *Macroscopic Field*

The time-dependent induced density is not the only source of the electromagnetic fields. In large systems, the induced current density also con-

tributes considerably. Therefore, we also have to consider the induced vector potential $\delta\mathbf{A}(\mathbf{r},t)$ which is defined within the Coulomb gauge according to,

$$\delta\mathbf{A}(\mathbf{r},t) = \frac{1}{c}\int \frac{\delta\mathbf{j}_T(\mathbf{r}',t-|\mathbf{r}-\mathbf{r}'|/c)}{|\mathbf{r}-\mathbf{r}'|}d\mathbf{r}'. \tag{10}$$

Here $\delta\mathbf{j}_T(\mathbf{r},t)$ is the induced transverse current density. This vector potential accounts, apart from the properly retarded contribution of the total induced current, also for the retardation effects which have not been included in the instantaneous Coulomb potential [38]. We can not neglect these retardation effects since the macroscopic part contains important contributions from remote regions. As we did for the density and the Coulomb potential, we have to distinguish microscopic and macroscopic contributions of the induced current density to this vector potential. We can safely ignore the microscopic part, because its electric field contribution is already a factor ω^2/c^2 in order smaller than that of the microscopic Coulomb potential. We will only have to retain the macroscopic part. This part is sample-shape dependent just like the macroscopic scalar potential.

We obtain the total macroscopic field from,

$$\mathbf{E}_{mac}(\mathbf{r},t) = \mathbf{E}_{ext}(\mathbf{r},t) - \frac{1}{c}\frac{\partial}{\partial t}\delta\mathbf{A}_{mac}(\mathbf{r},t) + \nabla\delta v_{mac}(\mathbf{r},t). \tag{11}$$

Here all macroscopic retardation effects are properly accounted for. The microscopic contribution to the field is completely described using the instantaneous microscopic Coulomb potential. This potential is lattice periodic and can therefore not contain any components that represent a macroscopic electric field. The field $\mathbf{E}_{mac}(\mathbf{r},t)$ of Eq. (11) is therefore indeed the macroscopic field of Eq. (1).

2.5. *Microscopic Coulomb Gauge*

We can now define a new gauge which we will call the microscopic Coulomb gauge. In this gauge the new scalar potential $\Phi'(\mathbf{r},t)$ is given by the instantaneous microscopic potential $\delta v_{mic}(\mathbf{r},t)$ of Eq. (6), while the associated vector potential $\mathbf{A}'(\mathbf{r},t)$ is fully retarded and completely specified by the macroscopic electric field $\mathbf{E}_{mac}(\mathbf{r},t)$ of Eq. (11)

$$\Phi'(\mathbf{r},t) = -\delta v_{mic}(\mathbf{r},t) \tag{12}$$

$$\mathbf{A}'(\mathbf{r},t) = -c\int^t \mathbf{E}_{mac}(\mathbf{r},t')\,dt'. \tag{13}$$

In the definition of these potentials we have neglected the microscopic retardation and microscopic magnetic effects. This is consistent with the neglect of the Breit corrections [39] in ground-state calculations.

The problems posed by the sample-shape dependence of the macroscopic field are circumvented by prescribing the total macroscopic electric field in the bulk as being uniform. We explicitly leave the surface region and sample shape undefined. We then only have to obtain the microscopic Coulomb potential of the periodic system in order to completely describe the fields in the bulk region.

The main conclusion of this analysis is that in the long-wavelength limit it suffices to know the induced lattice-periodic density and the induced macroscopic current density in the bulk for a given uniform macroscopic electric field in order to obtain the bulk-intrinsic induced microscopic potential and macroscopic polarization.

3. Time-Dependent Current-Density Functional Approach

We can now treat the dynamic linear response of a crystal to a fixed macroscopic field, within the idealized periodic boundary approximation. We use the perturbation approach to time-dependent density functional theory (TDDFT), in which both scalar and vector potentials are used to describe the perturbation. In its most general form this theory states that all observable quantities are functionals of both the time-dependent particle density $\rho(\mathbf{r},t)$ and the current density $\mathbf{j}(\mathbf{r},t)$. Ghosh and Dhara [25] have shown that this time-dependent density and current density can be constructed using a generalization of the effective one-electron scheme of Kohn and Sham [2]. In this scheme the single-particle wave functions $\psi_n(\mathbf{r},t)$ are solutions of the following time-dependent Schrödinger-type equation,

$$i\frac{\partial}{\partial t}\psi_n(\mathbf{r},t) = \left(\frac{1}{2}\left|-i\nabla + \frac{1}{c}\mathbf{A}_{\mathit{eff}}(\mathbf{r},t)\right|^2 + v_{\mathit{eff}}(\mathbf{r},t)\right)\psi_n(\mathbf{r},t), \qquad (14)$$

for suitably chosen initial conditions. The particles move in time-dependent effective potentials $\{v_{\mathit{eff}}(\mathbf{r},t), \mathbf{A}_{\mathit{eff}}(\mathbf{r},t)\}$, which are (in principle) uniquely determined (apart from an arbitrary gauge transform) by the exact time-dependent density and current density. These exact time-dependent densi-

ties follow from the solutions $\psi_n(\mathbf{r},t)$ via,

$$\rho(\mathbf{r},t) = \sum_{n=1}^{N} |\psi_n(\mathbf{r},t)|^2, \tag{15}$$

and,

$$\mathbf{j}(\mathbf{r},t) = \sum_{n=1}^{N} \Re\left\{-i\psi_n^*(\mathbf{r},t)\nabla\psi_n(\mathbf{r},t)\right\} - \frac{1}{c}\rho(\mathbf{r},t)\mathbf{A}_{\mathit{eff}}(\mathbf{r},t). \tag{16}$$

The first and second term on the right-hand side of Eq. (16) are the paramagnetic and diamagnetic currents respectively. The initial ground-state configuration is obtained by occupying only those one-electron states, which have evolved from the N solutions that are lowest in energy for the stationary state.

The effective potentials are the result of the externally applied potentials supplemented by internal contributions of the density and current distributions. In addition to the classical potentials of the charge and current densities, the latter also contain contributions that account for exchange and correlation effects. These exchange-correlation potentials are universal functionals of the charge and current density. Like in the original Kohn-Sham scheme, these effective potentials have to be obtained self-consistently. We can split up these potentials as follows

$$v_{\mathit{eff}}(\mathbf{r},t) = v_{mic}(\mathbf{r},t) + v_{xc,mic}[\rho,\mathbf{j}](\mathbf{r},t). \tag{17}$$

$$\mathbf{A}_{\mathit{eff}}(\mathbf{r},t) = -c\int^{t} [\mathbf{E}_{mac}(\mathbf{r},t') + \mathbf{E}_{xc}[\rho,\mathbf{j}](\mathbf{r},t')]dt'. \tag{18}$$

Note that we work in the microscopic Coulomb gauge not just for the classical components, but now for the effective potentials as well. Consequently we can regard $v_{\mathit{eff}}(\mathbf{r},t)$ as being lattice periodic. Due to the same reasoning, all macroscopic components of the effective scalar potential, also of the exchange-correlation contribution, should be combined with the effective vector potential. These give rise to an electric exchange-correlation field,

$$\mathbf{E}_{xc}[\rho,\mathbf{j}](\mathbf{r},t) = -\frac{1}{c}\frac{\partial}{\partial t}\mathbf{A}_{xc}[\rho,\mathbf{j}](\mathbf{r},t) + \nabla v_{xc,mac}[\rho,\mathbf{j}](\mathbf{r},t). \tag{19}$$

It remains to find good approximations for these exchange-correlation contributions.

As a first attempt we will assume that the microscopic component of the exchange-correlation scalar potential is an instantaneous functional of

just the periodic density. For the microscopic xc potential we will use the same functional dependence on the periodic density as in the ground state calculation, which is known as the adiabatic local density approximation (ALDA),

$$v_{xc,mic}^{ALDA}[\rho](\mathbf{r},t) = \left.\frac{d\left(\rho\epsilon_{xc}^{hom}(\rho)\right)}{d\rho}\right|_{\rho=\rho(\mathbf{r},t)}, \tag{20}$$

where $\epsilon_{xc}^{hom}(\rho)$ is the exchange-correlation energy density of the homogeneous electron gas. Again we will neglect any microscopic component of the effective vector potential. Moreover, all macroscopic components of the exchange-correlation contribution, which correspond to the macroscopic exchange-correlation electric field of Eq. (19), will not be taken into account. We will re-examine this approximation in Section 7. Within this approximation the effective vector potential becomes entirely defined by the macroscopic electric field via Eq. (13),

$$\mathbf{A}_{\mathit{eff}}(\mathbf{r},t) = \mathbf{A}'(\mathbf{r},t) = -c\int^{t}\mathbf{E}_{mac}(\mathbf{r},t')dt'. \tag{21}$$

With both effective potentials $v_{\mathit{eff}}(\mathbf{r},t)$ and $\mathbf{A}_{\mathit{eff}}(\mathbf{r},t)$ now properly defined, this completes the time-dependent self-consistency scheme.

3.1. *Linear Response*

For the calculation of linear response properties we only need to treat the time-dependent components of the density, current density, and potentials as first-order perturbations. First we obtain the ground-state density $\rho_0(\mathbf{r})$ and the ground state effective scalar potential $v_{\mathit{eff},0}(\mathbf{r})$ of this generalized Kohn-Sham problem. In the absence of any time-dependent macroscopic field this is an ordinary ground-state calculation. We then define the perturbation of the ground-state density by $\delta\rho(\mathbf{r},t) = \rho(\mathbf{r},t) - \rho_0(\mathbf{r})$. The change in the effective scalar potential $\delta v_{\mathit{eff}}(\mathbf{r},t) = v_{\mathit{eff}}(\mathbf{r},t) - v_{\mathit{eff},0}(\mathbf{r})$ comprises two contributions,

$$\delta v_{\mathit{eff}}(\mathbf{r},t) = \delta v_{mic}(\mathbf{r},t) + \delta v_{xc,mic}[\rho](\mathbf{r},t). \tag{22}$$

The classical part of this potential, i.e., the induced microscopic scalar potential $\delta v_{mic}(\mathbf{r},t)$, follows directly from Eq. (6). The first-order correction

to the exchange-correlation potential, $\delta v_{xc}[\rho](\mathbf{r},t)$, is formally defined using the (universal) exchange-correlation kernel $f_{xc}(\mathbf{r},t;\mathbf{r}',t')$,

$$\delta v_{xc,mic}[\rho](\mathbf{r},t) = \int^t \int f_{xc}[\rho_0](\mathbf{r},t;\mathbf{r}',t')\delta\rho(\mathbf{r}',t')\,d\mathbf{r}'\,dt'. \tag{23}$$

This kernel is the functional derivative of the time-dependent $v_{xc,mic}[\rho](\mathbf{r},t)$ with respect to the time-dependent density $\rho(\mathbf{r}',t')$. In the adiabatic local-density approximation the exchange-correlation kernel takes the form,

$$f_{xc}^{ALDA}[\rho_0](\mathbf{r},\mathbf{r}',t-t') = \delta(t-t')\delta(\mathbf{r}-\mathbf{r}')\left.\frac{d^2\left(\rho\epsilon_{xc}^{hom}(\rho)\right)}{d\rho^2}\right|_{\rho=\rho_0(\mathbf{r})}, \tag{24}$$

where the exchange-correlation energy density $\epsilon_{xc}^{hom}(\rho)$ of the homogeneous electron gas can be modeled for instance using the Vosko-Wilk-Nussair [40] parameterization.

The induced density has to be obtained self-consistently. We do this in an iterative way, in which the macroscopic field $\mathbf{E}_{mac}(t)$ is kept fixed while the induced effective potential $\delta v_{\mathit{eff}}(\mathbf{r},t)$ is updated in each cycle using the perturbed density of the previous cycle. This procedure is repeated until it has converged sufficiently.

The perturbation of the ground state which is due to the presence of the fixed uniform electric field and the induced scalar potential is governed by the perturbation Hamiltonian $\delta\hat{h}_{\mathit{eff}}$, which is given by,

$$\delta\hat{h}_{\mathit{eff}}(\mathbf{E}_{mac},\mathbf{r},t) = -\int^t \hat{\mathbf{j}}\cdot\mathbf{E}_{mac}(t')\,dt' + \delta v_{\mathit{eff}}(\mathbf{r},t). \tag{25}$$

Here only terms linear in the field have been retained. This perturbation is no longer a simple multiplicative operator like in ordinary TDDFT, since the macroscopic field couples to the (paramagnetic) current operator. This operator is defined as $\hat{\mathbf{j}} = -i(\nabla - \nabla^\dagger)/2$, where the dagger indicates that terms to the left have to be differentiated.

It is more convenient to go to the frequency domain to obtain an expression for the perturbed density. Using linear response theory, we get the induced density in first order,

$$\delta\rho(\mathbf{r},\omega) = \int\left(\frac{i}{\omega}\chi_{\rho\mathbf{j}}(\mathbf{r},\mathbf{r}',\omega)\cdot\mathbf{E}_{mac}(\omega) + \chi_{\rho\rho}(\mathbf{r},\mathbf{r}',\omega)\delta v_{\mathit{eff}}(\mathbf{r}',\omega)\right)d\mathbf{r}', \tag{26}$$

where the Kohn-Sham response functions $\chi_{\rho\rho},\chi_{\rho\mathbf{j}}(\mathbf{r},\mathbf{r}',\omega)$ are properties of the ground state. For periodic systems the ground-state solutions are

characterized by Bloch functions $\psi_{n\mathbf{k}}$ having energies $\epsilon_{n\mathbf{k}}$. They are counted by their integer band index n and continuous Bloch vector $\mathbf{k}$. The various Kohn-Sham response functions can be obtained from the occupied (i) and virtual (a) states of the ground-state system. They can be evaluated using the general form, valid for lattice-periodic perturbations,

$$\chi_{ab}(\mathbf{r},\mathbf{r}',\omega) = \frac{V}{4\pi^3}\sum_{i,a}\int \frac{\mathbf{a}_{ia\mathbf{k}}(\mathbf{r})\,\mathbf{b}^*_{ia\mathbf{k}}(\mathbf{r}')}{\epsilon_{i\mathbf{k}}-\epsilon_{a\mathbf{k}}+\omega+i\eta}\,d\mathbf{k} + c.c.(-\omega), \tag{27}$$

by substituting for $\mathbf{a}_{ia\mathbf{k}}(\mathbf{r})$ and $\mathbf{b}_{ia\mathbf{k}}(\mathbf{r})$ either the transition density $\rho_{ia\mathbf{k}}(\mathbf{r}) = \psi^*_{i\mathbf{k}}(\mathbf{r})\psi_{a\mathbf{k}}(\mathbf{r})$ or the transition current $\mathbf{j}_{ia\mathbf{k}}(\mathbf{r})$, which is given by,

$$\mathbf{j}_{ia\mathbf{k}}(\mathbf{r}) = -\frac{i}{2}\left(\psi^*_{i\mathbf{k}}(\mathbf{r})\nabla\psi_{a\mathbf{k}}(\mathbf{r}) - (\nabla\psi^*_{i\mathbf{k}}(\mathbf{r}))\psi_{a\mathbf{k}}(\mathbf{r})\right). \tag{28}$$

The positive infinitesimal η results from the adiabatic onset of the perturbation, and ensures causality. Note that, since the perturbations are all lattice periodic, we only have to include those contributions in the response kernel that conserve the Bloch vector $\mathbf{k}$.

The induced current density can be obtained as soon as self-consistency is established. Correct up to first order we obtain an expression similar to Eq. (26) for the paramagnetic current,

$$\delta\mathbf{j}_p(\mathbf{r},\omega) = \int\left(\frac{i}{\omega}\chi_{\mathbf{jj}}(\mathbf{r},\mathbf{r}',\omega)\cdot\mathbf{E}_{mac}(\omega) + \chi_{\mathbf{j}\rho}(\mathbf{r},\mathbf{r}',\omega)\delta v_{e\!f\!f}(\mathbf{r}',\omega)\right)d\mathbf{r}'. \tag{29}$$

It is important to note that the macroscopic field also contributes in first order via the diamagnetic contribution to the current,

$$\delta\mathbf{j}_d(\mathbf{r},\omega) = \frac{i}{\omega}\rho_0(\mathbf{r})\mathbf{E}_{mac}(\omega). \tag{30}$$

The induced current density is lattice-periodic, so that the macroscopic polarization is uniform and can be obtained from either Eq. (2) or (3) in their Fourier representations,

$$\mathbf{P}_{mac}(\omega) = \chi_e(\omega)\cdot\mathbf{E}_{mac}(\omega) = \frac{i}{V\omega}\int_V\left(\delta\mathbf{j}_p(\mathbf{r},\omega)+\delta\mathbf{j}_d(\mathbf{r},\omega)\right)d\mathbf{r}. \tag{31}$$

During the self-consistent field cycles it is convenient to set the macroscopic field to $\mathbf{E}_{mac}(\omega) = -i\omega\,\mathbf{e}_j$, i.e., to a field linear in ω and directed along a unit vector $\mathbf{e}_j$ and thus avoid the singularities at $\omega = 0$ in Eq. (26) and Eq. (29). The particular ω-dependence is not relevant since all induced quantities are linear in $\mathbf{E}_{mac}$. Note that $\mathbf{E}_{mac}(\omega) = \mathbf{E}^*_{mac}(-\omega)$, so that this

choice represents a real-valued electric field. This particular choice is equivalent to choosing a frequency-independent value for the vector potential, $\mathbf{A}'(\omega) = \mathbf{e}_j$. The diamagnetic contribution $\delta\mathbf{j}_d(\mathbf{r},\omega)$ that has to be added to the induced paramagnetic density of Eq. (29) to get the physical current then becomes frequency-independent, and, by using the conductivity sum rule, reduces to

$$\delta\mathbf{j}_d(\mathbf{r},\omega) = \delta\mathbf{j}_d(\mathbf{r},0) = -\delta\mathbf{j}_p(\mathbf{r},0). \tag{32}$$

The Cartesian components of the susceptibility then follow from Eq. (31),

$$[\chi_e(\omega)]_{ij} = \left\{ -\frac{1}{V\omega^2} \int_V [\delta\mathbf{j}_p(\mathbf{r},\omega) - \delta\mathbf{j}_p(\mathbf{r},0)]_i \, d\mathbf{r} \right\} \Bigg|_{\mathbf{E}_{mac}(\omega) = -i\omega\, \mathbf{e}_j} . \tag{33}$$

There is a definite numerical advantage in rewriting the expression in this way. The diamagnetic and paramagnetic parts are treated on equal footing, hence a proper behavior for the static limit $\omega \to 0$ is ensured.

4. Real-Space Implementation

The formulation in real space rather than in reciprocal space becomes feasible by solving the self-consistent field equations using an iterative scheme. This has some nice implications for the implementation. We do not have to construct the Kohn-Sham response kernels as such, but we will only have to evaluate them when constructing the response to a given perturbation. We will outline this approach here. Since the response kernels factorize according to Eq. 27, we can write the various contributions to the induced density and current, generically denoted by the property $\mathbf{a}(\mathbf{r},\omega)$, that result from the perturbing fields $\mathbf{E}_{\mathit{eff}}(\mathbf{r},\omega)$ and $v_{\mathit{eff}}(\mathbf{r},\omega)$, generically denoted by the field $\mathbf{F}(\mathbf{r},\omega)$, as follows,

$$\begin{aligned} \mathbf{a}(\mathbf{r},\omega) &= \int \chi_{ab}(\mathbf{r},\mathbf{r}',\omega) \cdot \mathbf{F}(\mathbf{r}',\omega) d\mathbf{r}' \\ &= \frac{V}{4\pi^3} \sum_{i,a} \int \mathbf{a}_{ia\mathbf{k}}(\mathbf{r}) \frac{\int \mathbf{b}^*_{ia\mathbf{k}}(\mathbf{r}') \cdot \mathbf{F}(\mathbf{r}',\omega) d\mathbf{r}'}{\epsilon_{i\mathbf{k}} - \epsilon_{a\mathbf{k}} + \omega + i\eta} \, d\mathbf{k} + c.c.(-\omega), \end{aligned} \tag{34}$$

where $\mathbf{a}_{ia\mathbf{k}}(\mathbf{r})$ and $\mathbf{b}_{ia\mathbf{k}}(\mathbf{r})$ are the transition density $\rho_{ia\mathbf{k}}(\mathbf{r})$ or the transition current $\mathbf{j}_{ia\mathbf{k}}(\mathbf{r})$. The integrals involving the field $\mathbf{F}(\mathbf{r},\omega)$ can be evaluated first, and serve as expansion coefficients $F_{ia\mathbf{k}}(\omega)$ in the construction of the induced $\mathbf{a}(\mathbf{r},\omega)$ from the transition elements $\mathbf{a}_{ia\mathbf{k}}(\mathbf{r})$. The $\mathbf{k}$-space integration involves the singular energy-dependent denominator. This singularity

is most easily treated in a Lehmann-Taut tetrahedron integration scheme [41]. We can generate a special quadrature by including the denominator in the integration weights according to,

$$\int \frac{d\mathbf{k}}{\epsilon_{i\mathbf{k}} - \epsilon_{a\mathbf{k}} + \omega + i\eta} = \int \frac{d\epsilon}{\epsilon + \omega + i\eta} \int d\mathbf{k}\, \delta(\epsilon - (\epsilon_{i\mathbf{k}} - \epsilon_{a\mathbf{k}})). \tag{35}$$

Given the energy dispersion of the ground state this yields a surface integration in $\mathbf{k}$-space. For these integrations standard ways to generate ϵ-dependent weights $\tilde{w}_{ia\mathbf{k}_n}(\epsilon)$ exist [42], defining the following numerical integration scheme,

$$\int d\mathbf{k}\, \delta(\epsilon - (\epsilon_{i\mathbf{k}} - \epsilon_{a\mathbf{k}})) f(\mathbf{k}) = \sum_{\mathbf{k}_n} \tilde{w}_{ia\mathbf{k}_n}(\epsilon) f(\mathbf{k}_n), \tag{36}$$

in which $\mathbf{k}_n$ are the integration points and the $\tilde{w}_{ia\mathbf{k}_n}(\epsilon)$ have a polynomial dependence on ϵ. We can now get a quadrature for the response kernels by performing the ϵ-integration analytically, defining new ω-dependent weights according to,

$$w_{ia\mathbf{k}_n}(\omega) = \int_{\epsilon_0}^{\epsilon_1} \frac{\tilde{w}_{ia\mathbf{k}_n}(\epsilon)}{\omega - \epsilon + i\eta} d\epsilon = \mathcal{P} \int_{\epsilon_0}^{\epsilon_1} \frac{\tilde{w}_{ia\mathbf{k}_n}(\epsilon)}{\omega - \epsilon} d\epsilon + i\pi\, \tilde{w}_{ia\mathbf{k}_n}(\omega). \tag{37}$$

The real and imaginary parts of these weights can thus be obtained separately using the Cauchy principle value and residual parts. The expansion for $\mathbf{a}(\mathbf{r}, \omega)$ now reads,

$$\mathbf{a}(\mathbf{r}, \omega) = \sum_{ia\mathbf{k}_n} w_{ia\mathbf{k}_n}(\omega) F_{ia\mathbf{k}_n}(\omega)\, \mathbf{a}_{ia\mathbf{k}_n}(\mathbf{r}), \tag{38}$$

which is just slightly more complicated than, for instance, the construction of the ground-state density.

For the evaluation of the microscopic Coulomb potential of the induced density we can use the same techniques as employed in the ground-state calculation for the deformation density. The induced density is mapped onto an auxiliary basis of fitfunctions $\{f_i(\mathbf{r})\}$ that have the appropriate symmetry. The fitset is constructed in such a way that the Coulomb integrals can be evaluated analytically, leading to the set of potentialfunctions $\{g_i(\mathbf{r})\}$. This is accomplished by using Bloch sums of one-center Slater type orbitals. With the expansion of $\delta\rho(\mathbf{r}, \omega)$ being given as $\delta\rho(\mathbf{r}, \omega) = \sum_i c_i(\omega) f_i(\mathbf{r})$, we can obtain the effective scalar potential from,

$$\delta v^{ALDA}_{eff,mic}(\mathbf{r}, \omega) = \sum_i c_i(\omega) g_i(\mathbf{r}) + f_{xc}^{ALDA}(\rho_0(\mathbf{r})) \delta\rho(\mathbf{r}, \omega). \tag{39}$$

The self-consistent field calculation proceeds as follows: given a start-up value for the induced effective potential, e.g., the uncoupled case $\delta v_{eff}(\mathbf{r}, \omega) = \mathbf{0}$, we can obtain the matrix elements for the perturbation, and, with them, the induced density from Eq. (38). Using the fitting procedure, we obtain the new Coulomb contribution to the effective potential, and, from the density itself, the exchange-correlation contribution Eq. (39). This completes the first cycle of the SCF scheme, and we iterate until convergence is reached. As convergence criterion we use the maximum change in the fitting coefficients for subsequent cycles, which must become negligible in order to reach convergence. All in all, the response calculation for a fixed frequency is comparable in computational cost as an ordinary ground state calculation. The same spatial resolution and accuracy is obtained for the induced density as for the ground-state density.

5. Application to Nonmetallic Binary Crystals

We have applied the TDDFT calculation scheme to a wide variety of nonmetallic crystals. In this section we focus on the isotropic elemental and binary semiconductors and insulators that have the diamond, rocksalt, or zincblende lattice structure.

The calculations were performed using the ADF-BAND (Refs. [32,33]) program. We made use of frozen cores and a hybrid valence basis consisting of the numerical atomic orbitals (NAO) of a free-atom Herman-Skillman (HS) program [43], in combination with Slater-type one-center functions (STO). The spatial resolution of this basis is equivalent to a triple-zeta STO basis that is augmented with two polarization functions. This valence basis was orthogonalized to the core states. The free-atom effective potential was provided by the same HS program. For the evaluation of the Coulomb integrals we used a single auxiliary basis of STO functions to represent the deformation density in the ground-state calculation as well as the induced density in the response calculation.

All matrix elements were evaluated numerically using an efficient and accurate quadrature scheme [32,44]. The numerical integration scheme for the **k**-space integrals used up to 175 symmetry-unique sample points in the irreducible wedge of the Brillouin zone. All results shown here were obtained using the Vosko-Wilk-Nusair parameterization [40] of the LDA exchange-correlation potential, which was also used to derive the ALDA exchange-correlation kernel.

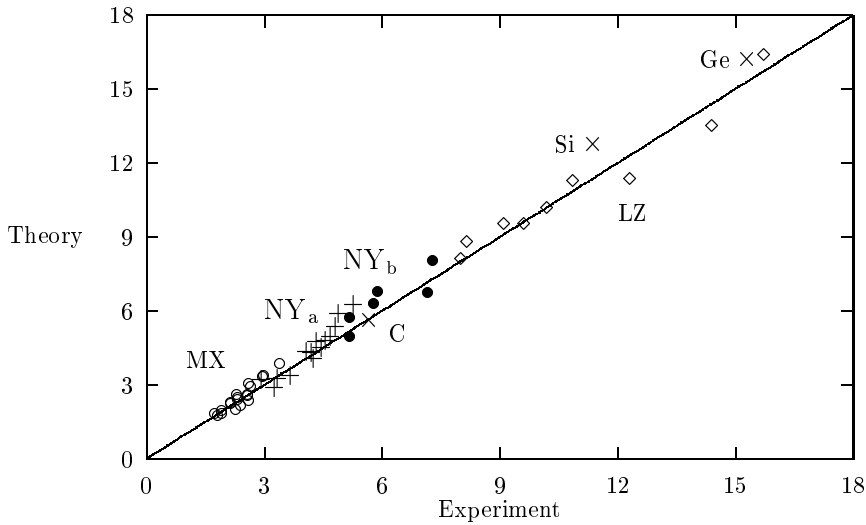

Fig. 2. Theoretical versus experimental dielectric constant for various elementary and binary crystals. The sodium chloride crystals (○) of the I-VI type MX (M=Li, Na, K, Rb, Cs; X=F, Cl, Br, I) and (+) of the II-VI type NY$_a$ (N=Mg, Ca, Sr, Ba; Y=O, S, Se, Te). The crystals in the diamond structure (×) (C, Si, Ge) and in the zincblende structure (◇) for the III-V type LZ (L=Al, Ga, In; Z=P, As, Sb) and (•) for the II-VI type NY$_b$ (N=Zn, Cd; Y=S, Se, Te).

5.1. *Dielectric Constants*

The binary compounds we have studied range from the ionic I-VII type to the more covalent III-V type, The most ionic materials occur in the rock-salt structure, whereas the more covalent materials occur in the zincblende structure. The transition in preferred structure occurs for the II-VI type, which contains crystals of both lattice type. The general trend found is that the higher the ionicity, the larger the Kohn-Sham gap is and the smaller the susceptibility becomes. In Fig. 2 we have compiled the results for the static dielectric constants ϵ_∞ for this large set of compounds. The materials have been grouped according to the chemical groups of the constituent elements as well as to their lattice type. For the whole range of materials we see a very good agreement of the TDDFT-ALDA calculations with experiment, with maximum deviations in the order of about 5%. Even though the LDA yields Kohn-Sham gaps that underestimate the experimental (charge)-gap

by about 40%-50% we do not systematically overestimate the dielectric constant.

We have also investigated the effect on the dielectric constant of the induced Coulomb and exchange-correlation contributions to the self-consistent potential. The uncoupled result can be obtained by setting $\delta v_{eff}(\mathbf{r}, \omega)$ equal to zero, which yields the bare response of the Kohn-Sham system. The coupled results have been obtained with and without inclusion of the exchange-correlation contribution. By including only the Coulomb contribution in the SCF procedure, the static value drops, e.g. in silicon, by about 25% relative to the bare response, Similar shifts, though smaller in magnitude, have been obtained in the dielectric matrix methods [7,8,16,31]. Including the exchange-correlation contribution in the coupled response raises the value again, relative to the Coulomb-only value by about 10%, We can conclude that the Coulomb interaction and exchange-correlation effects combined contribute considerably to the dielectric response, and that they are in the order of about 10%-15%. In some cases, e.g. in CaF_2 [45], we find major qualitative changes in the frequency dependence of the dielectric function due to the coupling.

5.2. *Dielectric Functions*

For a selected range of materials we have obtained the dielectric function $\epsilon(\omega)$. For the two most studied elemental materials, silicon and diamond, these are depicted in Fig. 3. All results have been obtained by including the Coulomb interaction and exchange-correlation effects (ALDA) in the SCF procedure. The algorithm used ensures that the real and imaginary parts form exact Kramers-Kronig pairs. The overall correspondence with experiment is reasonably good, in particular for the low frequency ranges. The sharp features in the spectra are reasonably well reproduced, except the first (E_1) peak of Silicon, which appears rather as a shoulder. These features can be attributed to the van Hove-type singularities in the joint-density of states, as obtained from the Kohn-Sham band structure. They appear at energies which are uniformly shifted downwards with respect to the experiments by, respectively, about 1.0 eV and 0.5 eV for C and Si. The calculated absorption edges coincide with the vertical Kohn-Sham energy gap of, respectively, 5.6 eV and 2.6 eV. In accordance with the general trend found in LDA calculations for the underestimation of the charge gap, we get more-or-less uniformly shifted absorption spectra for other materials too.

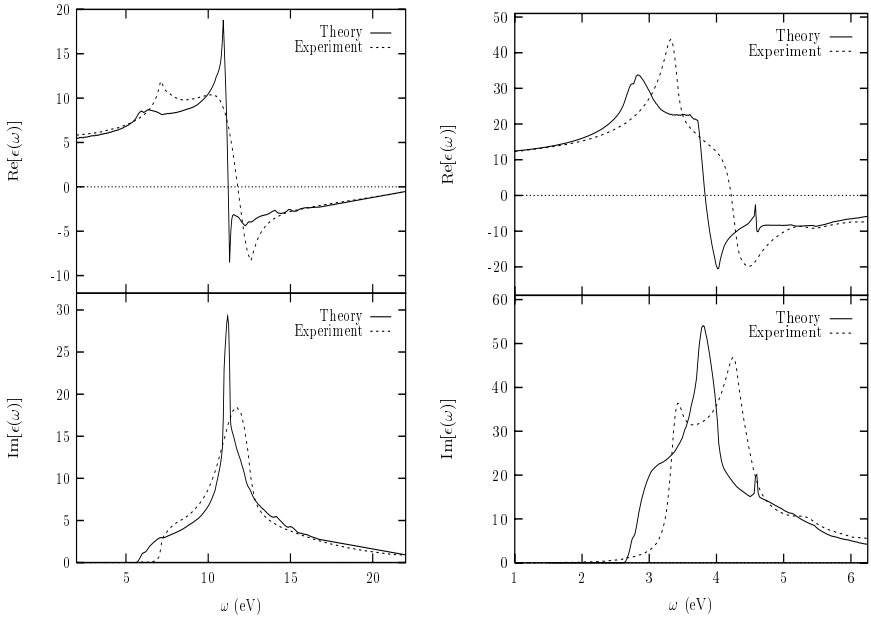

Fig. 3. The real (top) and imaginary (bottom) part of the calculated dielectric function for diamond (left) and silicon (right). The experimental data have been obtained from P. E. Aspnes and A. A. Studna, *Phys. Rev.* **B27**, 985 (1983).

However, there does not seem to be a one-to-one correspondence between the gap mismatch and the shifts needed to get good overall agreement. Here the criterion for the shifts was to bring the frequencies at which the real part changes sign in theory and experiment together. In Fig. 4 we show the spectra for two zincblende materials, gallium arsenide and zinc selenide, where this shift is applied. We get excellent overall agreement for the spectral features.

6. Relativistic Effects in the Response of Semimetals

Within the framework of ground-state density functional theory (DFT), scalar relativistic effects can be treated using the zeroth order regular approximation (ZORA) [46,47,48]. In this approach the kinetic energy operator $p^2/2$ is replaced by its ZORA-equivalent, resulting in the following Kohn-

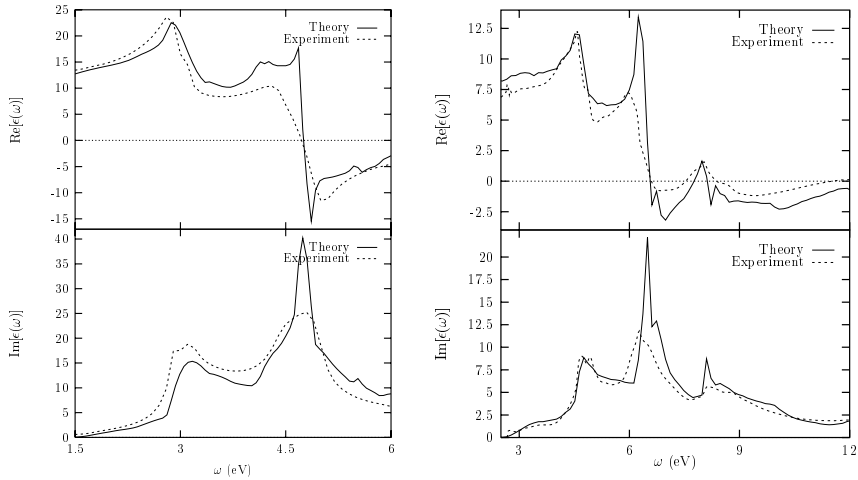

Fig. 4. The real (top) and imaginary (bottom) part of the dielectric function for gallium arsenide (left) and zinc selenide (right). The experimental data have been obtained from P. E. Aspnes and A. A. Studna, *Phys. Rev.* **B27**, 985 (1983) and J. L. Freelouf. *Phys. Rev.* **B7**, 3810 (1973). The spectra have been shifted over 0.45 eV and 1.05 eV for GaAs and ZnSe respectively to facilitate the comparison

Sham equation,

$$\left[\mathbf{p}\cdot\frac{c^2}{2c^2-v_{\mathit{eff}}(\mathbf{r})}\mathbf{p}+v_{\mathit{eff}}(\mathbf{r})\right]\psi_{n\mathbf{k}}(\mathbf{r})=\epsilon_{n\mathbf{k}}\psi_{n\mathbf{k}}(\mathbf{r}). \tag{40}$$

Here $\mathbf{p}=-i\nabla$ is the momentum operator, c the velocity of light, and $v_{\mathit{eff}}(\mathbf{r})$ the self-consistent effective scalar potential.

The time-dependent Kohn-Sham system in the presence of an electromagnetic field is now described by a Hamiltonian that is obtained by replacing the ground state momentum operator $\mathbf{p}$ by $\mathbf{p}=-i\nabla+1/c\,\mathbf{A}_{\mathit{eff}}(\mathbf{r},t)$, and the effective scalar potential $v_{\mathit{eff}}(\mathbf{r})$ by the time-dependent version $v_{\mathit{eff}}(\mathbf{r},t)=v_{\mathit{eff},0}(\mathbf{r})+\delta v_{\mathit{eff}}(\mathbf{r},t)$. Within the same order of regular approximation, we can neglect the additional time-dependent contribution to the scalar potential that appears in the denominator of the ZORA kinetic energy term of Eq. 40.

We can now proceed along the same lines as in the nonrelativistic case, and introduce the linear response equations analogous to Eqs. 26 and 29. The scalar relativistic effects enter the response calculations by modifying the Kohn-Sham response kernels of Eq. 27 in three different ways. Most

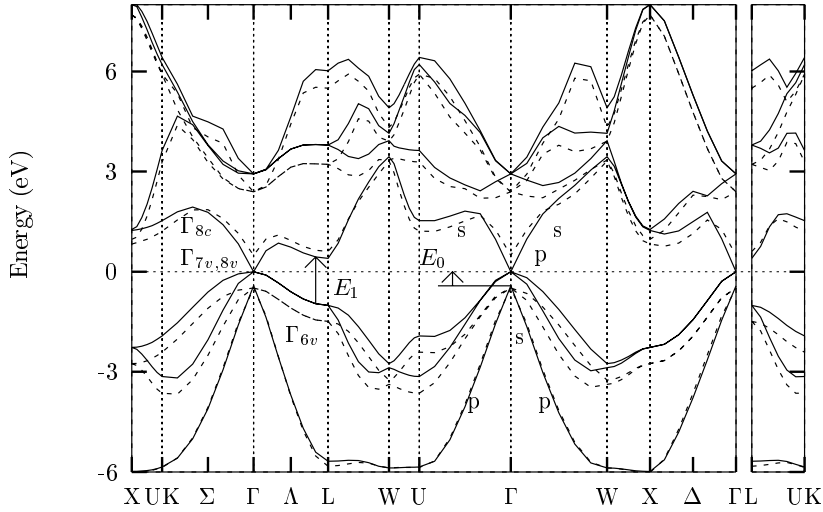

Fig. 5. The inverted band structure of InSb. The solid line is the result with scalar relativistic effects included. The dashed line is the nonrelativistic ground-state calculation. Critical points E_0 and E_1 and the band character (s or p) are indicated near the zone center Γ.

importantly, the response kernels will change through the modification of the Kohn-Sham energies on one hand and the wavefunctions that describe the ground state on the other. There is however a third relativistic effect, namely through the modification of the relativistic transition current $\mathbf{j}_{ia\mathbf{k}}(\mathbf{r})$, which now becomes defined by [34],

$$\mathbf{j}_{ia\mathbf{k}}(\mathbf{r}) = \frac{-ic^2}{2c^2 - v_{eff}(\mathbf{r})} \left(\psi^*_{i\mathbf{k}}(\mathbf{r})\nabla\psi_{a\mathbf{k}}(\mathbf{r}) - (\nabla\psi^*_{i\mathbf{k}}(\mathbf{r}))\psi_{a\mathbf{k}}(\mathbf{r})\right). \qquad (41)$$

The two materials which we want to discuss here, InSb and HgSe, become semimetallic within the ZORA-LDA approximation, as result of the inversion of their bandstructures at the center of the Brillouin zone. This phenomenon is depicted in Fig. 5 for the InSb case. A very similar behavior is found for HgSe. In both cases, the s-like states at the conduction band minimum are stabilized with respect to the p-like states at the valence band maximum, which is mainly due to the relativistic mass-velocity effect. The inversion of the typical band order of zincblende type semiconductors results in an inverted gap with an avoided crossing, even at high symmetry

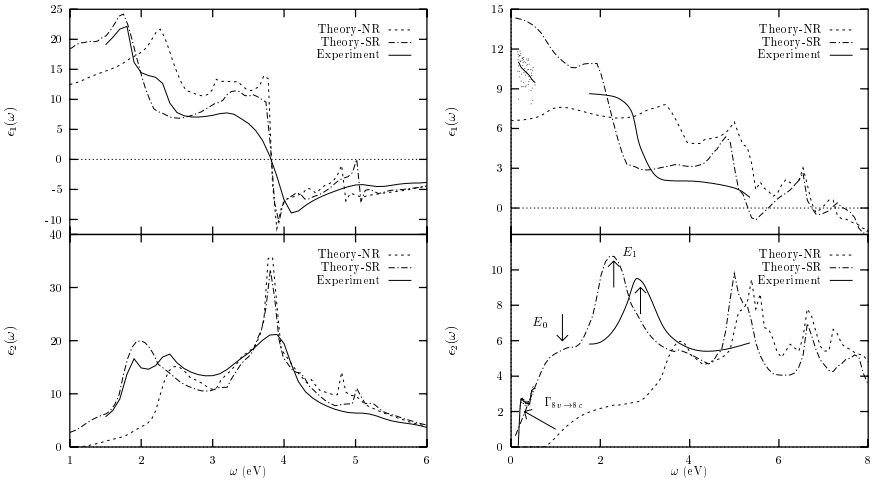

Fig. 6. Plots of the real and imaginary part (top and bottom) of the calculated dielectric function of InSb and HgSe (right and left). The results with and without scalar relativistic effects (SR, dash-dotted line, respectively NR, dotted line) are compared with experimental data. For HgSe these have been compiled from S. Einfeldt *et al. Phys. Rev.* **B51**, 4915 (1995), and K. Kumazaki *et al. Solid State Commun.* **68**, 591 (1988) (dots and solid line). For InSb these data have been obtained from P. E. Aspnes and A. A. Studna, *Phys. Rev.* **B27**, 985 (1983). The calculated spectra of InSb have been shifted over 0.30 eV (SR) and 0.15 eV (NR) respectively.

.

directions, since the s-like band hybridizes with one of the p-like valence bands. The transition between the bands connecting to the degenerate Γ_{8v} and Γ_{8c}, is symmetry forbidden at Γ, but becomes allowed outside this point. There Γ_{8c} changes character rapidly from p- to s-like, and simultaneous with the changing of Γ_{8c} the band connecting to Γ_{6v} changes from s- to p-character. The bands connecting to Γ_{8v} and Γ_{7v} remain of p-character.

The absence of the energy gap in the ground-state calculation and the quadratic dispersion of the valence and conduction bands make it necessary to investigate the small-frequency behavior for the Kohn-Sham response kernels. It turns out that these kernels do not show any singular behavior, as can be shown in a careful symmetry and $\mathbf{k}\cdot\mathbf{p}$ analysis [34]. Our TDDFT results [34,35] for the spectra of the dielectric functions are depicted in Fig. 6. In both cases we see a drastic change with the inclusion of the scalar relativistic effects. Upon the inclusion of these effects, the ϵ_∞ changes from

9.15 to 16.42 in InSb (15.7 experimentally [49]), and in HgSe from 6.6 to 14.4 (11.7 experimentally [35]). Hence we get good overall agreement with experiment, where in particular the static value and the relative peak positions and peak heights are greatly improved.

7. Beyond the (Adiabatic) Local Density Approximation

The results presented in the preceding sections were all obtained using the adiabatic local density approximation for the exchange and correlation (xc) effects. Here we want to go beyond the adiabatic approximation. However, the formulation of a local dynamical approximation for the xc potential turns out to be extremely difficult, because within TDDFT such a potential is an intrinsically nonlocal functional of the density (i.e., there does not exist a gradient expansion for the frequency-dependent xc potential in terms of the density alone). Vignale and Kohn [37,50] were the first to formulate a local gradient expansion in terms of the *current density*. In a time-dependent current density functional approach to linear response theory, they derived an expression for the linearized xc vector potential $\mathbf{a}_{\rm xc}(\mathbf{r},\omega)$ for a system of slowly varying density, subject to a spatially slowly varying external potential at a finite frequency ω.

One can write this functional in the compact form derived by Vignale, Ullrich and Conti [51],

$$E_{xc}[\rho_0,\mathbf{j}](\mathbf{r},\omega) = \frac{-1}{\rho_0(\mathbf{r})}\nabla\cdot\sigma_{xc}[\rho_0,\mathbf{j}](\mathbf{r},\omega). \tag{42}$$

Here $E_{xc}(\mathbf{r},\omega)$ is the induced xc-electric field in linear response. Within the microscopic gauge this field has to be combined with the first order change in the xc-potential $v^{\rm ALDA}_{xc,mic}(\mathbf{r},\omega)$ which has to be evaluated in the adiabatic local density approximation (ALDA). The electric field term contains the ground state density $\rho_0(\mathbf{r})$ of the system and the symmetric viscoelastic stress tensor, which is defined through its components according to

$$\begin{aligned}\sigma_{xc,ij}[\rho_0,\mathbf{j}](\mathbf{r},\omega) = \tilde{\eta}_{xc}(\rho_0(\mathbf{r}),\omega)\left(\nabla_j u_i + \nabla_i u_j - \frac{2}{3}\delta_{ij}\nabla\cdot\mathbf{u}\right)(\mathbf{r},\omega)\\ +\tilde{\zeta}_{xc}(\rho_0(\mathbf{r}),\omega)\delta_{ij}\nabla\cdot\mathbf{u}(\mathbf{r},\omega).\end{aligned} \tag{43}$$

Here $\mathbf{u}(\mathbf{r},\omega) = \delta\mathbf{j}(\mathbf{r},\omega)/\rho_0(\mathbf{r})$ is the induced velocity field and the functions $\tilde{\eta}_{xc}(\rho_0,\omega)$ and $\tilde{\zeta}_{xc}(\rho_0,\omega)$ are the coefficients of elasticity and viscosity which can be expressed in terms of the transverse and longitudinal xc kernels of the electron gas [51], $f_{xcT}(\rho,\omega)$ and $f_{xcL}(\rho,\omega)$ respectively.

7.1. *Polarization Functional*

Let us first look at the consequences of such an exchange-correlation field. In order to isolate the macroscopic component of this field, we can take the average over a unit cell of the solid. If, in addition, we neglect all microscopic variation of the induced current density, the rather complicated functional dependence is reduced and can be written in a simple form [36],

$$\mathbf{E}_{xc,mac}(\omega) = \frac{i}{\omega}\mathbf{Y}[\rho_0](\omega)\cdot\delta\mathbf{j}(\omega) = \mathbf{Y}[\rho_0](\omega)\cdot\mathbf{P}_{mac}(\omega), \tag{44}$$

where the tensor $\mathbf{Y}[\rho_0](\omega)$ is a property of the ground state which is given by,

$$\mathbf{Y}_{ij}[\rho](\omega) = \frac{1}{\Omega}\int_{\Omega}\frac{\nabla_i\rho\,\nabla_j\rho}{\rho^2}(\mathbf{r})\left(\delta_{ij}f_{xcT}(\rho(\mathbf{r}),\omega) + h_{xc}(\rho(\mathbf{r}),\omega)\right)d\mathbf{r}. \tag{45}$$

Here $h_{xc}(\rho,\omega)$ is given as,

$$h_{xc}(\rho,\omega) = f_{xcL}(\rho,\omega) - f_{xcT}(\rho,\omega) - \frac{d^2(\rho\epsilon_{xc}^{hom}(\rho))}{d\rho^2}, \tag{46}$$

with $\epsilon_{xc}^{hom}(\rho)$ the xc-energy density of the homogeneous electron gas. Equation (44) represents the first explicit example of the often discussed density-polarization functional [19,52,53]. With this polarization functional we can proceed as follows. If we consider the macroscopic effective field as the parameter of the usual response calculation we obtain the Kohn-Sham response function $\tilde{\chi}(\omega)$ by,

$$\mathbf{P}_{mac}(\omega) = \tilde{\chi}(\omega)\cdot\mathbf{E}_{\mathit{eff}}(\omega) = \tilde{\chi}(\omega)\cdot\left(\mathbf{E}_{mac}(\omega) + \mathrm{Y}(\omega)\cdot\mathbf{P}_{mac}(\omega)\right). \tag{47}$$

The true electric susceptibility $\chi_e(\omega)$ that relates $\mathbf{P}_{mac}(\omega)$ to the macroscopic field $\mathbf{E}_{mac}(\omega)$ then follows from,

$$\chi_e(\omega) = (1 - \tilde{\chi}(\omega)\mathbf{Y}(\omega))^{-1}\tilde{\chi}(\omega). \tag{48}$$

This equation clearly displays the influence of the macroscopic xc-electric field on the susceptibility. It remains to find appropriate approximations for the functions f_{xcT} and f_{xcL}.

7.2. *Results*

The transverse and longitudinal response functions have been investigated in detail for the electron gas [54,55,56,57]. In these works it has been shown that they are smooth functions of the frequency, except at twice the plasma

frequency. For the optical spectra we are, however, interested in much smaller frequencies. In the limit $\omega \to 0$ the function $h_{xc}(\rho_0, \omega)$ reduces to $f_{xcT}(\rho_0, 0)/3$ [51]. In that limit the tensor $\mathbf{Y}[\rho](0)$ is completely determined by $f_{xcT}(\rho, 0)$. We obtain values for $f_{xcT}(\rho_0, 0)$ at arbitrary ρ_0, by using a cubic spline interpolation based on the tabulated values of Ref. [56] in which we take into account the exactly known high density behavior [57].

The optical absorption spectrum ϵ_2 for Si, shows two major peaks in the range from 3-6 eV. All previous 'one-electron' approximations, ranging from the early pseudopotential approaches in the 70's [58,59], to the *ab initio* DFT-LDA of the end 90's [60], showed the same features for ϵ_2. However, the E_1 peak is usually underestimated, and appears just as a shoulder, which is attributed to the neglect of excitonic effects [61] (the attractive interaction between the virtual hole and the excited electron).

The ratio of the E_1-E_2 peak heights in the calculated ϵ_2 of Si proved to be rather sensitive to the numerical value of $\mathbf{Y}([\rho_0], 0)$. As it turns out, the theoretical value that we obtain for $\mathbf{Y}([\rho_0], 0)$ is too high, and we have to introduce a scaling of 0.4 in order to get an optimal agreement with experiment for the ratio of the E_1-E_2 peak heights. This scaling may be the result of the neglect of all microscopic contributions to the exchange-correlation field and the uncertainty in the tabulated values of $f_{xcT}(\rho_0, 0)$ [57]. As can be seen in Fig. 7, for both the real and imaginary part of $\epsilon(\omega)$, the whole dielectric function is improved considerably upon inclusion of this polarization functional. It is clear that without the $\mathbf{E}_{\mathrm{xc,mac}}$ contributions, the E_1 peak appears as a shoulder and is underestimated in amplitude, while the E_2 peak is too sharp, and therefore overestimated in magnitude. When including the macroscopic xc-contributions, the E_1 peak is now clearly resolved, while the E_2 peak is hardly affected.

The same prefactor is used in various other cases too. In the same figure we show the effect of including the polarization functional for diamond and gallium phosphide. Clearly there is a very small effect on ϵ_2 in diamond when using the polarization functional, whereas in gallium phosphide the originally underestimated E_1 peak is now found in full agreement with experiment,

8. Conclusions

In this article we reviewed the time-dependent current density functional approach for the description of the dielectric properties of crystalline solids.

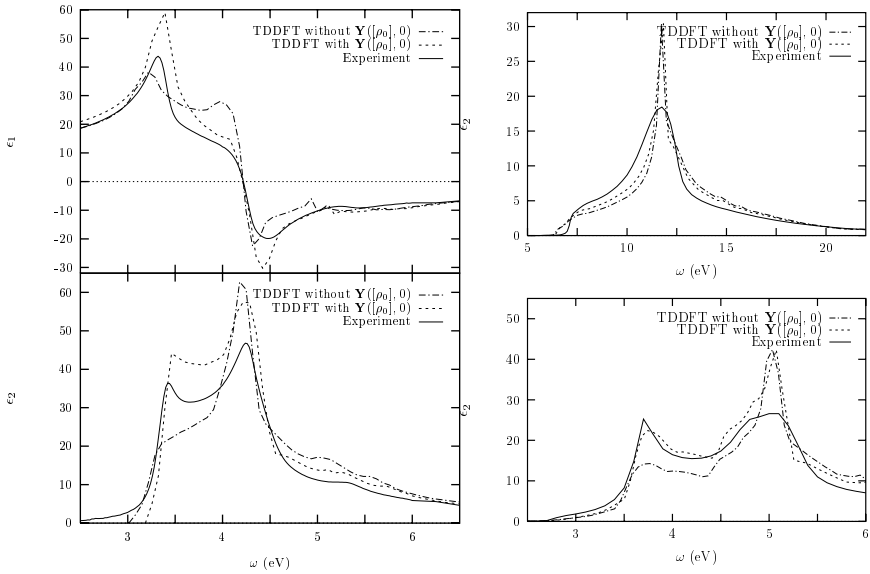

Fig. 7. The real and imaginary part of the dielectric function for silicon (top and bottom of left panel), without and with inclusion of the polarization dependent functional, together with experimental data. The energy shifts applied to the TDDFT calculated dielectric function were 0.60 eV without, and 0.70 eV with the inclusion of $\mathbf{Y}(0)$. Similar results for the absorption of diamond (top right, shift of 0.40 eV resp. 0.58 eV) and gallium phosphide (bottom right, shift of0.5 eV resp. 0.6 eV)

We showed that the treatment of solids in the presence of time-dependent electromagnetic fields using lattice periodic model systems requires the combination of uniform electric fields with lattice periodic effective potentials. The electric susceptibility can then be obtained if the macroscopic polarization is derived from the spatially averaged induced current density. We used a perturbative approach to the time-dependent self-consistent field scheme, for which we derived a real space description. We outlined the efficient iterative approach for the solution of this calculation scheme, which has been implemented in a full-potential code that uses a linear combination of atomic orbitals as basis.

The results were presented for the dielectric constants of a variety of elemental and binary compounds. For a selection of these materials we also obtained the dielectric function. Already within the adiabatic density approximation we get good agreement with experiment. In particular good

results are obtained for the dielectric constant, where we achieve an accuracy of about 5%. Exchange and correlation effects contribute up to 15% to the electric susceptibility. The spectral features are reproduced well, but they appear at energies that are nearly rigidly shifted towards lower energies.

The method proved also to be successful for the description of the semimetallic zincblende materials InSb and HgSe, which have inverted band-structures within the local density approximation due to relativistic effects. We observed drastic effects on the dielectric properties which were greatly improved upon the inclusion of scalar relativistic effects. As a first attempt to go beyond the adiabatic local density approximation, we tried a polarization functional that was derived from the current density exchange-correlation functional of Vignale and Kohn [37]. We get improved results for the absorption spectra of various semiconductors when including the exchange-correlation contributions to the electric field using this functional.

Acknowledgments

The authors would like to acknowledge H. Aissa and J. A. Berger for their valuable contributions to the implementation of the relativistic effects and the polarization dependent functional into the ADF-BAND response code.

References

1. P. Hohenberg and W. Kohn, *Phys. Rev.* **B136**, 864 (1964).
2. W. Kohn and L. J. Sham, *Phys. Rev.* **A140**, 1133 (1965).
3. R. O. Jones and O. Gunnarsson, *Rev. Mod. Phys.* **61**, 689 (1989).
4. E. J. Baerends, D. E. Ellis, and P. Ros, *Chem. Phys.* **2**, 41 (1973).
5. R. M. Dreizler and E. K. U. Gross, *Density Functional Theory; An Approach to the Quantum Many-Body Problem* (Springer-Verlag, Berlin, 1990).
6. R. G. Parr and W. Yang, *Density Functional Theory of Atoms and Molecules*, (Oxford University Press, Oxford, 1990).
7. S. Baroni and R. Resta, *Phys. Rev.* **B33**, 7017 (1986).
8. Z. H. Levine and D. C. Allan, *Phys. Rev.* **B43**, 4187 (1991); **44**, 12781 (1991); *Phys. Rev. Lett.* **63**, 1719 (1989); **66**, 41 (1991).
9. A. Zangwill and P. Soven, *Phys. Rev.* **A21**, 1561 (1980).
10. R. van Leeuwen and E. J. Baerends, *Phys. Rev.* **A49**, 2421 (1994).
11. S. J. A. van Gisbergen, V. P. Osinga, O. V. Gritsenko, R. van Leeuwen, J. G. Snijders, and E. J. Baerends, *J. Chem. Phys.* **105**, 3142 (1996).
12. M. S. Hybertsen and S. G. Louie, *Phys. Rev.* **B30**, 5777 (1984).
13. A. Dal Corso, S. Baroni, and R. Resta, *Phys. Rev.* **B49**, 5323 (1994).

14. L. J. Sham and M. Schlüter, *Phys. Rev. Lett.* **51**, 1888 (1983); *Phys. Rev.* **B32**, 3883 (1965).
15. J. P. Perdew and M. Levy, *Phys. Rev. Lett.* **51**, 1884 (1983).
16. M. S. Hybertsen and S. G. Louie, *Phys. Rev.* **B34**, 5390 (1986).
17. R. W. Godby, M. Schlüter, and L. J. Sham, *Phys. Rev. Lett.* **56**, 2415 (1986); *Phys. Rev.* **B37** 10159 (1988).
18. J. Chen, Z. H. Levine, and J. W. Wilkins, *Phys. Rev.* **B50**, 11514 (1994).
19. X. Gonze, P. Ghosez, and R. W. Godby, *Phys. Rev. Lett.* **74**, 4035 (1995).
20. E. Runge and E. K. U. Gross, *Phys. Rev. Lett.* **52**, 997 (1984).
21. G. D. Mahan and K. R. Subbaswami, *Local Density Theory of Polarizability* (Plenum Press, New York, 1990).
22. E. K. U. Gross, C. A. Ullrich, and U. J. Gossmann, in *Density Functional Theory*, Ed. E. K. U. Gross and R. M. Dreizler, (Plenum Press, New York, 1995), p. 149ff.
23. S. J. A. van Gisbergen, J. G. Snijders, and E. J. Baerends, *J. Chem. Phys.* **103**, 9347 (1995); *Comput. Phys. Commun.* **118**, 119 (1999).
24. A. K. Dhara and S. K. Ghosh, *Phys. Rev.* **A35**, 442 (1987).
25. S. K. Ghosh and A. K. Dhara, *Phys. Rev.* **A38**, 1149 (1988).
26. F. Kootstra, P. L. de Boeij, and J. G. Snijders, *J. Chem. Phys.* **112**, 6517 (2000).
27. F. Kootstra, P. L. de Boeij, and J. G. Snijders, *Phys. Rev.* **B62**, 7071 (2000).
28. S. Baroni, P. Giannozzi, and A. Testa, *Phys. Rev. Lett.* **58**, 1861 (1987).
29. S. L. Adler, *Phys. Rev.* **126**, 413 (1962).
30. N. Wiser, *Phys. Rev.* **129**, 62 (1963).
31. M. S. Hybertsen and S. G. Louie, *Phys. Rev.* **B35**, 5585 (1987); *ibid.* **35**, 5602 (1987).
32. G. te Velde and E. J. Baerends, *Phys. Rev.* **B44**, 7888 (1991); *J. Comput. Phys.* **99**, 84 (1992).
33. C. Fonseca Guerra, O. Visser, J. G. Snijders, G. te Velde, and E. J. Baerends, in *Methods and Techniques in Computational Chemistry*, Ed. E. Clementi and G. Corongiu, (STEF, Cagliary, 1995), p. 305; G. te Velde, F. M. Bickelhaupt, E. J. Baerends, C. Fonseca Guerra, S. J. A. van Gisbergen, J. G. Snijders, and T. Ziegler, *J. Comp. Chem.* **22**, 931 (2001).
34. F. Kootstra, P. L. de Boeij, H. Aissa, and J. G. Snijders, *J. Chem. Phys.* **114**, 1860 (2001).
35. P. L. de Boeij, F. Kootstra, and J. G. Snijders, *Int. J. Quantum Chem.* accepted.
36. P. L. de Boeij, F. Kootstra, J. A. Berger, R. van Leeuwen, and J. G. Snijders, *J. Chem. Phys.* accepted.
37. G. Vignale and W. Kohn, *Phys. Rev. Lett.* **77**, 2037 (1996).
38. O. L. Brill and B. Goodman, *Am. J. Phys.* **35**, 832 (1967).
39. G. Breit, *Phys. Rev.* **34**, 553 (1929); *ibid.* **39**, 616 (1932).
40. S. H. Vosko, L. Wilk, and M. Nusair, *Can. J. Phys.* **58**, 1200 (1980).

41. G. Lehmann and M. Taut, *Phys. Status. Solidi.* **B54**, 469 (1972).
42. G. Wiesenekker and E. J. Baerends, *J. Phys.: Condens. Matter* **3**, 6721 (1991); G. Wiesenekker, G. te Velde, and E. J. Baerends, *J. Phys.* **C21**, 4263 (1988).
43. F. Herman and S. Skillman, *Atomic Structure Calculations*, (Prentice-Hall, Englewood Cliffs NJ, 1963).
44. P. M. Boerrigter, G. te Velde, and E. J. Baerends, *Int. J. Quantum Chem.* **33**, 87 (1988).
45. F. Kootstra, P. L. de Boeij, R. van Leeuwen, and J. G. Snijders, *J. Chem. Phys.* to be published.
46. E. van Lenthe, E. J. Baerends, and J. G. Snijders, *J. Chem. Phys.* **101**, 9783 (1994).
47. E. van Lenthe, R. van Leeuwen, E. J. Baerends, and J. G. Snijders, *Int. J. Quantum Chem.* **57**, 281 (1996).
48. P. H. T. Philipsen, E. van Lenthe, J. G. Snijders, and E. J. Baerends, *Phys. Rev.* **B56**, 13556 (1997).
49. E. Burstein, H. Brodsky and G. Lucousky, Int. J. Quantum Chem. **1**, 756 (1967).
50. G. Vignale and W. Kohn, in *Electronic Density Functional Theory: Recent Progress and New Directions*, Ed. J. F. Dobson *et al.* , (Plenum Press, New York, 1998).
51. G. Vignale, C. A. Ullrich, and S. Conti, *Phys. Rev. Lett.* **79**, 4878 (1997).
52. X. Gonze, P. Ghosez, and R. Godby, *Phys. Rev. Lett.* **78**, 294 (1997).
53. R. M. Martin and G. Ortiz, *Phys. Rev.* **B56**, 1124 (1997).
54. H. M. Böhm, S. Conti, and M. P. Tosi, *J. Phys. Cond. Matter* **8**, 781 (1996).
55. S. Conti, R. Nifosi, and M. P. Tosi, *J. Phys. Cond. Matter* **9**, L475 (1997).
56. R. Nifosi, S. Conti, and M. P. Tosi, *Phys. Rev.* **B58**, 12758 (1998).
57. S. Conti and G. Vignale, *Phys. Rev.* **B60**, 7966 (1999).
58. D. J. Stukel, R. N. Euwema, T. C. Collins, F. Herman, and R. L. Kortum, *Phys. Rev.* **179**, 740 (1969).
59. J. P. Walter, M. L. Cohen, Y. Petroff, and M. Balkanski, *Phys. Rev.* **B1**, 2661 (1970).
60. V. I. Gravilenko and F. Bechstedt, *Phys. Rev.* **B54**, 13416 (1996).
61. S. Albrecht, L. Reining, R. Del Sole, and G. Onida, *Phys. Rev. Lett.* **80**, 4510 (1998).